Characterization of a Microstrip Line Referenced to a Meshed Return Plane Using 2-D Analysis

Ze Sun[®], *Member, IEEE*, Jian Liu, Xiaoyan Xiong, DongHyun Kim[®], *Member, IEEE*, Daryl Beetner[®], *Senior Member, IEEE*, and Victor Khilkevich[®], *Member, IEEE*

Abstract—Transmission lines with meshed return planes offer enhanced flexibility but can introduce signal integrity challenges. Characterizing such transmission lines using full-wave simulation is accurate but time and resource intensive. In response, an efficient modeling method using 2-D analysis is proposed in this article. First, cross sections of the transmission line are taken at multiple locations to create a sampled representation of the changing geometry. The per-unit-length (PUL) RLGC parameters of each segment are obtained using 2-D analysis. The value of the inductance obtained from the 2-D analysis is then modified to account for the position-dependent current direction on the return plane. Finally, the segments are cascaded together to obtain the S-parameters of the transmission line. The results obtained using this method closely align with those from 3-D full-wave simulations, demonstrating the effectiveness and efficiency of the proposed approach.

Index Terms—Mesh return plane, printed circuit board, signal integrity, transmission line.

I. INTRODUCTION

N MODERN compact electronic devices, flexible printed circuit boards (FPCBs) have become an essential component for achieving reliable and space-saving designs. The physical flexibility of these boards is made possible through the implementation of a meshed reference plane, which is significantly different from the traditional microstrip that employs a solid reference plane. The adoption of a meshed reference plane presents a set of challenges, including signal integrity issue like the variations in characteristic impedance along the signal trace [1], and the electromagnetic (EM) radiation [2] [3]. This article focuses on the characterization of signal integrity behavior in microstrip lines with meshed return plane.

Transmission lines with a solid reference plane can be modeled by 2-D cross-sectional analysis [4] [5] because the geometries are translationally invariant. When dealing with traces that reference to a meshed plane, however, the geometrical variations of the ground plane require the application of a full-wave simulation for accurate modeling. This requirement poses challenges

Manuscript received 28 June 2023; revised 23 September 2023; accepted 30 November 2023. Date of publication 5 December 2023; date of current version 27 December 2023. This work is supported by National Science Foundation under Grant IIP-1916535. (Corresponding author: Ze Sun.)

Ze Sun, DongHyun Kim, Daryl Beetner, and Victor Khilkevich are with the Missouri University of Science and Technology, Rolla, MO 65409 USA (e-mail: sunz1@umsystem.edu; kimdonghy@umsystem.edu; daryl@mst.edu; khilkevichv@mst.edu).

Jian Liu and Xiaoyan Xiong are with Cadence Design Systems Inc, San Jose, CA 95134-1931 USA (e-mail: jliu@cadence.com; xiongx@cadence.com). Digital Object Identifier 10.1109/TSIPI.2023.3339445

in terms of both time efficiency and computational resource consumption. For example, in [6], [7], and [8], the S-parameters of the transmission line needed to be obtained from full-wave simulation to extract the effective characteristic impedance and the per-unit-length (PUL) parameters.

To overcome these challenges, this research introduces a novel method for calculating the *S*-parameters of a single-ended trace referenced to a meshed return plane using only 2-D analysis. The proposed approach accounts for the periodic changes in the structure and the position-dependent direction of the current flow. The accuracy of this method was validated through comparison with full-wave simulation results.

This article is organized as follows. In Section II, the geometry sampling procedure is introduced. By extracting and simulating the cross-sectional geometries of the transmission line at various locations using a 2-D solver, the resulting RLGC parameters can be cascaded to obtain the S-parameter of the entire board. As will be shown, however, the 2-D analysis fails to capture the changes in return current flow direction caused by the geometry of the return plane, leading to inaccuracies in the resulting S-parameters.

The rest of this article is organized as follows: In Section II, the proposed modeling methodology is introduced. In Section III, a method is proposed to modify the calculated inductance of the return plane obtained by the 2-D analysis. By doing so, the current flow path around the mesh apertures can be handled correctly. In Section IV, the proposed method is applied to specific transmission line geometries for validation. Finally, Section V concludes this article.

II. PROPOSED MODELING METHOD: INITIAL APPROACH

In this section, the proposed modeling methodology is introduced. First, cross sections of the transmission line were taken at multiple locations along the trace to create a sampled representation of the changing geometry. It is critical to ensure that the distance between adjacent cuts is small relative to the size of the return plane aperture to enable appropriate sampling of the ground geometry. Next, 2-D EM analysis was performed using the cross-sectional geometries at the corresponding cuts to obtain the PUL RLGC parameters of each segment. The RLGC parameters can then be converted to matrix parameters (S or ABCD) by representing each segment as a translationally invariant transmission line with a length equal to the sampling step. Finally, the matrix parameters of the segments were cascaded to derive the matrix representation of the entire transmission line.

2768-1866 © 2023 IEEE. Personal use is permitted, but republication/redistribution requires IEEE permission. See https://www.ieee.org/publications/rights/index.html for more information.

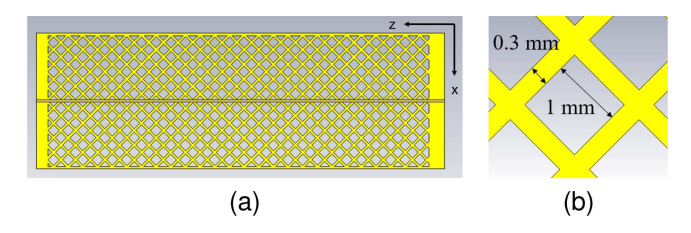


Fig. 1. (a) Top view of single-ended signal trace referenced to a meshed return plane. The x-axis is along the vertical direction, the z-axis is along the horizontal direction. (b) Zoom-in to the reference ground period.

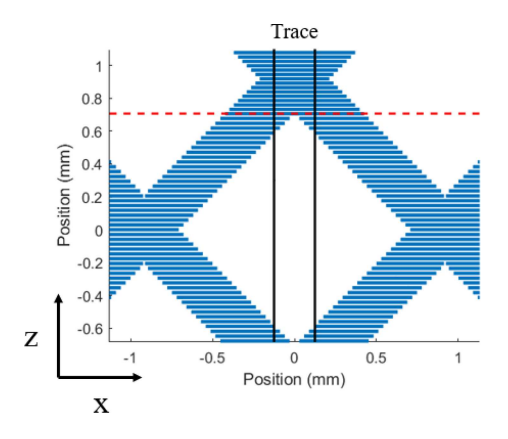


Fig. 2. Segmentation of the meshed round period. Only the portion closes to the signal trace is shown. The lower and higher portions of the lattice were divided by the red dashed line.

It has been observed, however, that this method cannot accurately model the transmission line. To demonstrate this, a simulated single-ended signal trace referenced to a meshed return plane was analyzed using a full-wave solver (CST [9]), as depicted in Fig. 1. The total length of the line was 51.24 mm, with a ground plane hatch width of 0.3 mm and a hatch pitch of 1 mm. To ensure continuity with the port modes, the reference plane on the left and right boundaries was solid, each with a length of 1.72 mm. The trace width and the air layer between the trace and reference plane were 0.25 and 0.08 mm, respectively, while the thicknesses of both the trace and reference plane were 0.03 mm. The center of the trace was aligned with the center of the return plane apertures. It took four and a half hours to complete the simulation on a server with Intel 6136 processor using the frequency domain solver.

Following the proposed methodology, the mesh period was cross-sectioned at 64 locations, as illustrated in Fig. 2. The geometry was sampled at a step of 29.5 μm below the dashed line and 26.5 μm above the line, respectively. The sampling steps were less than 2% of the lattice period (1.84 mm). This approach resulted in 49 cuts uniformly distributed around the aperture and 15 cuts uniformly distributed at the crosshatch intersection. The cuts were indexed in ascending order from the bottom to the top, with cut 1 and cut 49 located at the bottom and top vertices of the square hole, respectively, and cut 25 located in the center of the hole. Due to symmetry, the cross section at cut i was identical to cut 50 - i, where i was any integer between 1 and 24, and the cross section at cut i was identical to cut 114 - i, where i was any

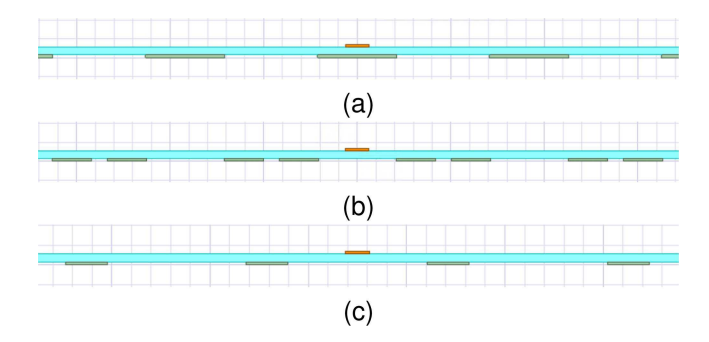


Fig. 3. Cross-sectional geometries at (a) cut 1, (b) cut 15, and (c) cut 25.

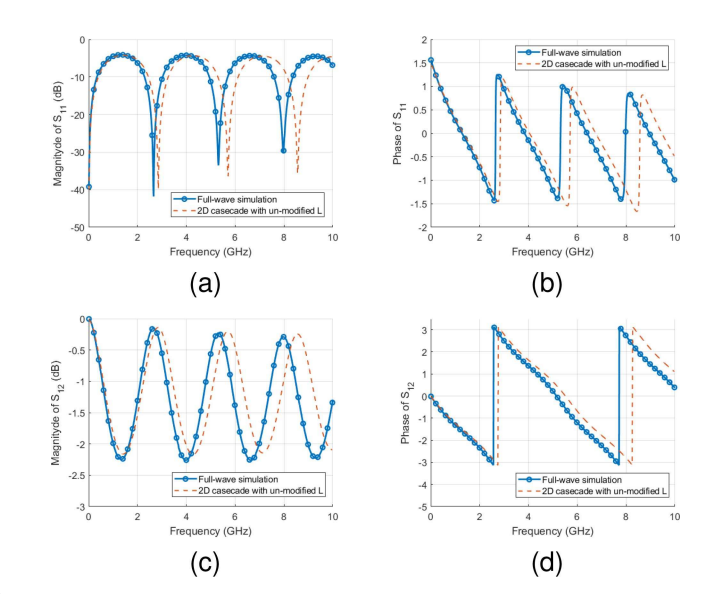


Fig. 4. Comparison between full-wave and segmented models. (a) Magnitude of S_{11} . (b) Phase of S_{11} . (c) Magnitude of S_{12} . (d) Phase of S_{12} .

integer between 50 and 56. This approach reduces the number of the required cross-sectional analyses to 33 instead of 64. Such cross-sectioning strategy, however, is not mandatory and does not limit the applicability of the method to nonsymmectrical geometries. The cross-sectional geometries of several cuts are depicted in Fig. 3. The RLGC parameters of each segment were simulated using the Ansys Q2D solver.

The S-parameters of one period can be calculated by cascading the RLGC parameters of the 64 segments together. After this, the S-parameters of the entire line in Fig. 1 were calculated by cascading 26 periods and the two solid return plane segments at the two ends. The comparison between the magnitude and phase of the transmission coefficient (normalized to 50 Ω) obtained by the full-wave solver and by cascading the segments is presented in Fig. 4. The disparity in the magnitude and phase of S_{12} obtained through these two methods was quantified by the relative errors defined as

$$\delta|S_{12}| = \frac{\||S_{12_{\text{cst}}}| - |S_{12_{\text{2.D}}}|\|}{\||S_{12_{\text{cst}}}\|}$$
(1)

$$\delta \arg S_{12} = \frac{\|\arg(S_{12_{\rm cst}}) - \arg(S_{12_{\rm 2-D}})\|}{\|\arg(S_{12_{\rm cst}})\|}.$$
 (2)

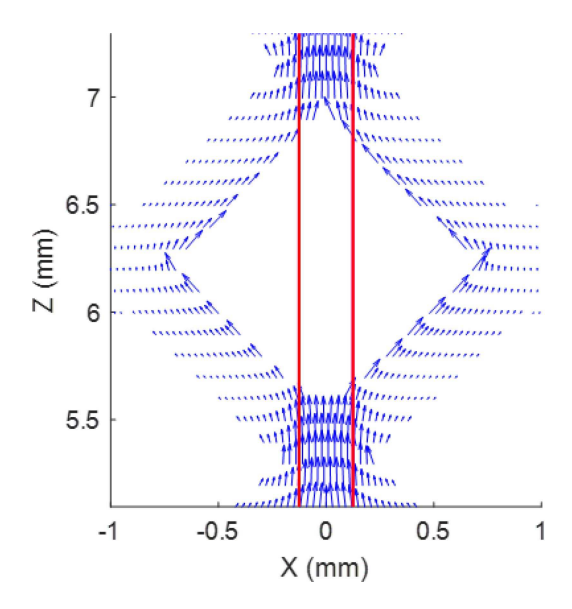


Fig. 5. Current density distribution on the top surface of the return plane. The vertical red lines indicate the position of trace.

The analysis revealed a relative error of 6.8% in magnitude and 6.6% in phase. As can be seen from Fig. 4(c), the lines models exhibit different electrical lengths, as evidenced by the phase progression. This discrepancy can lead to errors in the modeling of differential line skew [10]. The mismatch arises from errors in the calculation of inductance, which is discussed in Section III.

It should be noted that the presented method, based on cross-sectional analysis, implicitly assumes that only the transverse electromagnetic modes (TEM) exist in each cross section. In reality, this is, of course, not true, and the non-TEM modes are always present due to the nonuniformity of the transmission line ground. This means that the presented method should be seen as a low-frequency approximation, i.e., assuming that the size of the apertures in the ground plane is electrically small. As such, the possible EM interference caused by the ground plane is not modeled. In addition to that, the signal degradation at high frequencies caused by the significant non-TEM field at the apertures is not taken into account as well.

III. CURRENT FLOW PATH ON A MESHED RETURN PLANE

To investigate the error observed in the cascaded model, the surface current distribution on the return plane produced by the full-wave solver CST is shown in Fig. 5. The current flow direction on the meshed return plane is position-dependent. Specifically, when a conductor is located underneath the trace, the return current primarily flows along the z direction. In the absence of a ground conductor, the return current predominantly flows along the edges of the apertures in the meshed return plane. In the 2-D analysis, however, the information about the position-dependent return current direction is missing as the geometry of the return plane is assumed to be translationally invariant. As a result, the direction of the return current is always normal to the cross-sectional plane.

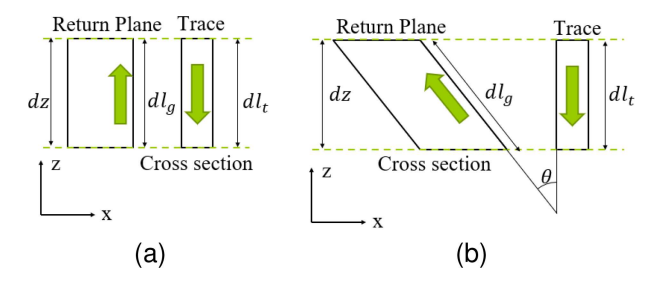


Fig. 6. (a) Assumed current flow direction in 2-D analysis. (b) Top view of current flow direction in a transmission line with a mesh return plane.

The difference in current flow direction between the 2-D and 3-D simulations is illustrated qualitatively in Fig. 6. For a segment of the translationally invariant line [Fig. 6(a)] with length dz, the length of both the trace and ground conductors is equal to the segment length: $dl_t = dl_g = dz$. In contrast, for the line with the meshed ground [Fig. 6(b)], the length of the conductor in which the current flows at an angle θ relative to the trace is longer: $dl_g = dz/\cos\theta$. This difference affect the inductance value. Therefore, the inductance value obtained from the 2-D simulation needs to be modified to account for the effect of the current flow direction, which is discussed in detail in Sections III-A to III-C.

It is important to note that the value of the PUL capacitance C is unaffected by the current flow direction, while the PUL resistance R is (because of the increased length of the return current path). The analysis presented in Fig. 4 highlights that the amplitude of the reflection and transmission coefficients is reproduced quite accurately even without modifying the PUL R of the segments, suggesting that the influence of the meshed ground plane on the conductor loss is a relatively weak effect. Therefore, this study primarily focuses on investigating the influence of the position-dependent current direction on the inductance value and correcting the phase progression; accurate modeling of the conductor loss is outside the scope of this article and could be a topic of future research.

A. Reconstruction of Return Current Direction

The 2-D analysis only provides the magnitude distribution of the current at the cross sections. To determine the modified inductance, however, it is necessary to reconstruct the current flow direction.

The governing equation for the current density \vec{J} on the return plane is the continuity equation [11]

$$\nabla \cdot \vec{J} = -\frac{\partial \rho}{\partial t} \tag{3}$$

where $\partial \rho / \partial t$ represents the rate of change of the charge density ρ , which is zero in the case of a transmission line.

The divergence of \vec{J} in (3) can be expressed as

$$\frac{\partial J_x}{\partial x} + \frac{\partial J_y}{\partial y} + \frac{\partial J_z}{\partial z} = 0.$$
 (4)

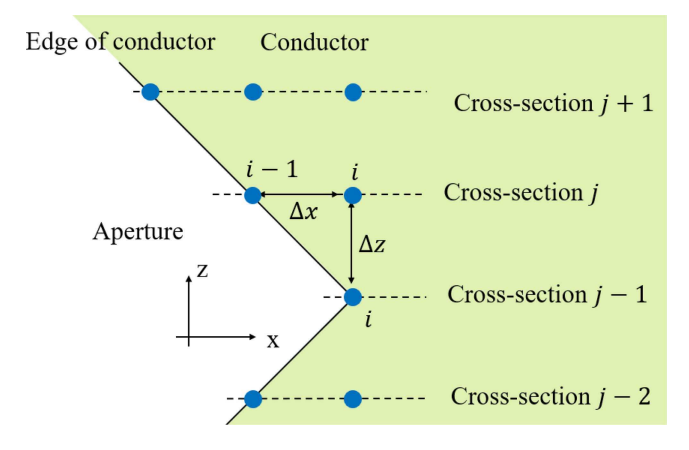


Fig. 7. Solving for the current flow direction using the finite difference.

Considering that the thickness of the return plane is much smaller compared to its width and length, the change in current density in the y direction can be neglected $\left(\frac{\partial J_y}{\partial y}=0\right)$. As depicted in Fig. 6(b), when the angle between the current flow direction and the z direction is denoted as θ , (4) can be rewritten as

$$\frac{\partial(-|\vec{J}|\sin\theta)}{\partial x} + \frac{\partial(|\vec{J}|\cos\theta)}{\partial z} = 0.$$
 (5)

Following the Leibniz product rule, the derivatives in the x and z directions can be expressed as

$$-|\vec{J}|\cos\theta \frac{\partial\theta}{\partial x} - \frac{\partial|\vec{J}|}{\partial x}\sin\theta - |\vec{J}|\sin\theta \frac{\partial\theta}{\partial z} + \frac{\partial|\vec{J}|}{\partial z}\cos\theta = 0.$$
 (6)

By dividing each term by $-|\vec{J}|$, (6) can be reformulated as

$$\left(M + \frac{\partial \theta}{\partial z}\right) \sin\theta + \left(\frac{\partial \theta}{\partial x} - N\right) \cos\theta = 0 \tag{7}$$

where M and N are normalized derivatives of the absolute value of the current density

$$M = \frac{\partial |\vec{J}|}{\partial x} / |\vec{J}| \tag{8}$$

$$N = \frac{\partial |\vec{J}|}{\partial z} / |\vec{J}|. \tag{9}$$

The tangent of the angle θ can be expressed from (7) as

$$\tan\theta = \frac{N - \frac{\partial\theta}{\partial x}}{M + \frac{\partial\theta}{\partial x}}.$$
(10)

Equation (10) is a nonlinear partial differential equation with respect to θ . The equation can be solved by meshing the geometry by a rectangular grid and substituting the partial derivatives with the finite differences [12]. An example of the meshing is shown in Fig. 7. From the 2-D analysis, the current amplitude $|\vec{J}_{ij}|$ is known at the points i in the cross sections j. Thus, the values of the functions M and N at a point (i,j) can be calculated, for example, as

$$M_{i,j} \approx \frac{|\vec{J}_{i,j}| - |\vec{J}_{i-1,j}|}{|\vec{J}_{i,j}|}, N_{i,j} \approx \frac{|\vec{J}_{i,j}| - |\vec{J}_{i,j-1}|}{\Delta z}.$$
 (11)

Similarly, the partial derivatives of the angle at the location (i, j) are calculated as

$$\frac{\partial \theta_{i,j}}{\partial x} \approx \frac{\theta_{i,j} - \theta_{i-1,j}}{\Delta x}, \frac{\partial \theta_{i,j}}{\partial z} \approx \frac{\theta_{i,j} - \theta_{i,j-1}}{\Delta z}.$$
 (12)

Finally, (10) can be rewritten in terms of the finite differences

$$\tan \theta_{i,j} = \frac{\frac{|\vec{J}_{i,j}| - |\vec{J}_{i,j-1}|}{\Delta z} - \frac{\theta_{i,j} - \theta_{i-1,j}}{\Delta x}}{\frac{|\vec{J}_{i,j}| - |\vec{J}_{i-1,j}|}{\Delta x}} + \frac{\theta_{i,j} - \theta_{i,j-1}}{\Delta z}.$$
(13)

The values of the angles at the boundary of each segment j (i.e., at the edges of the conductor) are known and are equal to the angle of the conductor edges relative to the z-axis. Therefore, (13) can be solved at each location (i,j) by specifying a certain angle for the current in the first segment (for example, the current can be set parallel to the z-axis) and then iteratively solving the equation at each point in the remaining cross sections.

B. Modifying Inductance Based on Current Flow Direction

After reconstructing the current flow direction, the inductance can be calculated based on the definition [13]

$$L = \frac{\Phi}{I} = \frac{\int_{S} \vec{B} \cdot d\vec{s}}{I} \tag{14}$$

where Φ is the magnetic flux through the surface S between the trace and the return plane. This quantity is determined by calculating the surface integral of the normal component of the magnetic field \vec{B} over the surface S. Beside, the magnetic field \vec{B} field can be computed as [14]

$$\vec{B} = \nabla \times \vec{A} \tag{15}$$

where \vec{A} denotes the vector potential. By substituting (15) into (14) and applying the Stokes's theorem, a representation of inductance can be derived in terms of \vec{A}

$$L = \frac{\oint_c \vec{A} \cdot d\vec{l}}{I}.$$
 (16)

In this equation, c refers to the closed contour encircling surface S. The inductance can be divided into contributions from the trace and the return plane, thus, (16) can be reformulated as

$$L = L_{\text{trace}} + L_{\text{GND}} = \frac{\oint_{c} \vec{A}_{\text{trace}} \cdot d\vec{l}}{I} + \frac{\oint_{c} \vec{A}_{\text{GND}} \cdot d\vec{l}}{I}$$
(17)

where \vec{A}_{trace} and \vec{A}_{GND} represent the vector magnetic fields generated by the current flowing on the signal trace and on the return plane, respectively.

Let us first analyze the return conductor contribution $L_{\rm GND}$ in the infinitesimal segments of length dl formed by two parallel and nonparallel filament currents, as depicted in Fig. 8. When the return current is normal to the cross-sectional plane, the direction of $\vec{A}_{\rm GND}$ aligns with the z direction. The direction of the integral line is set as clockwise, and it can be separated into four segments: two segments parallel to the trace and return path (CD and AB), and two segments perpendicular to the trace and return path (BC and DA). As $\vec{A}_{\rm GND}$ is orthogonal to BC and

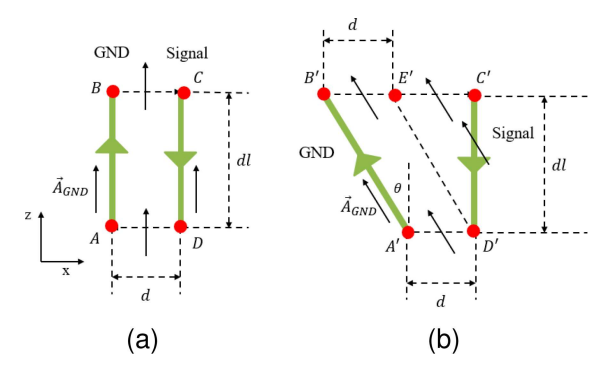


Fig. 8. Calculation of $L_{\rm GND}$ of segments formed by: (a) two parallel filament currents and (b) two nonparallel filament currents.

DA, the corresponding line integral is zero. Consequently, $L_{\rm GND}$ can be calculated as

$$L_{\text{GND}} = \frac{\int_A^B \vec{A}_{\text{GND}} \, d\vec{l} + \int_C^D \vec{A}_{\text{GND}} \, d\vec{l}}{I}.$$
 (18)

Since the lines in Fig. 8 are formed by infinitely long conductors and the length of the segment is infinitesimal, the vector potential is constant along the lines parallel to the conductors (i.e., $\vec{A}_{\text{GND}}(A) = \vec{A}_{\text{GND}}(B)$ and $\vec{A}_{\text{GND}}(C) = \vec{A}_{\text{GND}}(D)$) and the integrals in (18) can be replaced by products

$$L_{\text{GND}} = \frac{|\vec{A}_{\text{GND}}(A)|dl - |\vec{A}_{\text{GND}}(D)|dl}{I}.$$
 (19)

In the case of a meshed return plane, as depicted in Fig. 8(b), the direction of \vec{A}_{GND} remains parallel to the return current but no longer aligns with the z direction. An additional point E' is introduced between B' and C', such that |B'E'| = |D'A'|. This subdivision allows the line integral to be split into five segments. In this way, the line integral between B'E' and D'A' cancel with each other.

Therefore, similar to (19), the contribution of the return conductor L'_{GND} can be expressed as

$$L'_{\text{GND}} = \frac{1}{I} (|\vec{A}_{\text{GND}}(A')| \frac{dl}{\cos \theta} + \int_{E'}^{C'} \vec{A}_{\text{GND}} \, d\vec{l} + \int_{C'}^{D'} \vec{A}_{\text{GND}} \, d\vec{l})$$
(20)

where $\frac{dl}{\cos\theta}$ represents the length of the segment A'B'.

As the segment length dl is infinitesimal, the length of the segment E'C' is infinitesimal as well (if $\theta \neq \pi/2$) and the values of the magnetic potential at points E' and C' become equal, and both are in turn equal to the value at point D': $\vec{A}_{\rm GND}(E') = \vec{A}_{\rm GND}(C') = \vec{A}_{\rm GND}(D')$. In this case, the integrals along the paths E'D' and E'C'D' will be equal

$$\int_{E'}^{C'} \vec{A}_{\text{GND}} d\vec{l} + \int_{C'}^{D'} \vec{A}_{\text{GND}} d\vec{l}$$

$$= -|\vec{A}_{\text{GND}}(D')| dl \tan\theta \sin\theta - |\vec{A}_{\text{GND}}(D')| dl \cos\theta$$

$$= -|\vec{A}_{\text{GND}}(D')| \frac{dl}{\cos\theta} = \int_{E'}^{D'} \vec{A}_{\text{GND}} d\vec{l}.$$
(21)

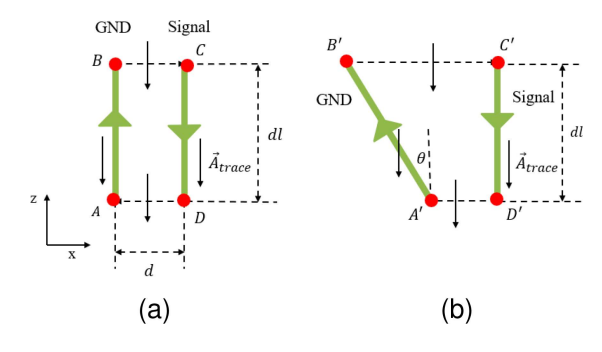


Fig. 9. Calculation of L_{trace} of segments formed by: (a) two parallel filament currents and (b) two nonparallel filament currents.

Substituting (21) into (20), L'_{GND} can be written as

$$L'_{\text{GND}} = \frac{\frac{dl}{\cos\theta}(|\vec{A}_{\text{GND}}(A')| - |\vec{A}_{\text{GND}}(D')|)}{I}.$$
 (22)

The magnitude of $\vec{A}_{\rm GND}$ depends on the distance between the observation point and the source current. In (18) and (22), it can be observed that $|\vec{A}_{\rm GND}(A)| = |\vec{A}_{\rm GND}(A')|$ and $|\vec{A}_{\rm GND}(D)| = |\vec{A}_{\rm GND}(D')|$. Therefore,

$$L'_{\text{GND}} = \frac{1}{\cos \theta} L_{\text{GND}}.$$
 (23)

The variation of $L_{\rm trace}$ for the meshed return plane case can be derived similarly. Fig. 9(a) displays the distribution of \vec{A} generated by the trace current for the parallel case. Same as Fig. 8(a), the integral line can be divided into four segments, and $L_{\rm trace}$ can be expressed as

$$L_{\text{trace}} = \frac{\oint_{c} \vec{A}_{\text{trace}} \cdot d\vec{l}}{I} = \frac{|\vec{A}_{\text{trace}}(D)| dl - |\vec{A}_{\text{trace}}(A)| dl}{I}. \quad (24)$$

For the case of the meshed return plane illustrated in Fig. 9(b), the direction of \vec{A}_{trace} aligns with the z direction. As a result, the modified inductance L'_{trace} is equal to L_{trace} for the parallel case, as follows:

$$L'_{\text{trace}} = \frac{\oint_{c} \vec{A} \cdot d\vec{l}}{I} = \frac{\int_{C'}^{D'} \vec{A}_{\text{trace}} d\vec{l} + \int_{A'}^{B'} \vec{A}_{\text{trace}} d\vec{l}}{I}$$

$$= \frac{|\vec{A}_{\text{trace}}(D)| dl - |\vec{A}_{\text{trace}}(A)| dl}{I} = L_{\text{trace}}. \tag{25}$$

By combining the contributions of $L_{\rm GND}$ and $L_{\rm trace}$, the corresponding PUL inductance should be modified as

$$L' = L_{\text{trace}} + \frac{1}{\cos \theta} L_{\text{GND}}.$$
 (26)

C. Calculating the PUL Inductance of the Cross Sections

At each cut, the reconstructed current flow direction is position-dependent. In order to modify the PUL L using (26), which describes the inductance of the filament currents, the sum of the filament current contributions needs to be taken [15], [16].

After reconstructing the return current density \vec{J} using the method discussed in Section III-A, the return current at each cut can be represented as a combination of multiple filaments. If the distance between two adjacent filaments is Δd , the current of the

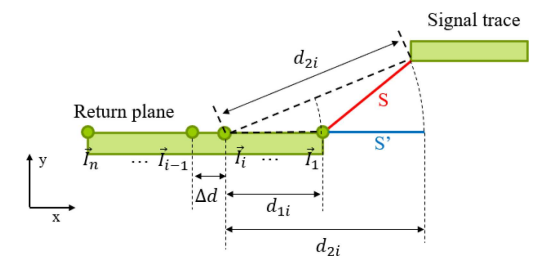


Fig. 10. Calculation of the magnetic flux of the return plane filament currents.

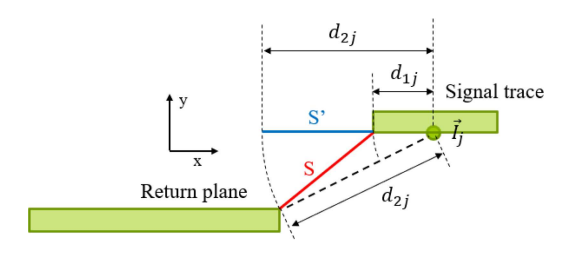


Fig. 11. Calculation of the magnetic flux of the trace filament currents.

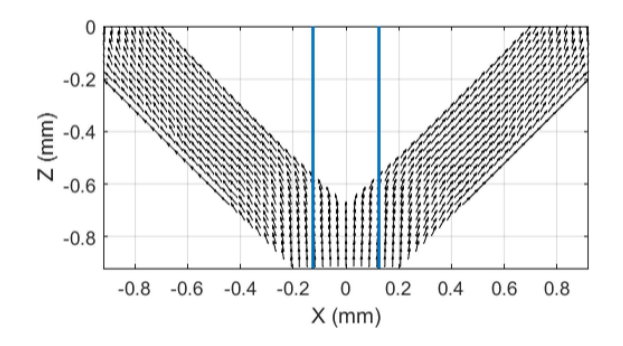


Fig. 12. Fragment of the reconstructed return current. The blue lines indicate the position of the signal trace. The arrows represent normalized current density vectors.

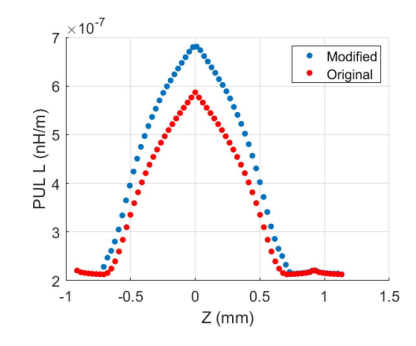


Fig. 13. PUL L of the segments before and after modification according to (32).

ith filament can be calculated as $\vec{I_i} = \Delta d\vec{J_i}$. In the case when the return current is parallel to the signal trace, as depicted in Fig. 10, the magnetic flux density $\vec{B_i}$ generated by the ith filament can be obtained using the Biot-Savart law as [17]

$$\vec{B_i} = \hat{e_\varphi} \frac{\mu_0 |\vec{I_i}|}{2\pi r} \tag{27}$$

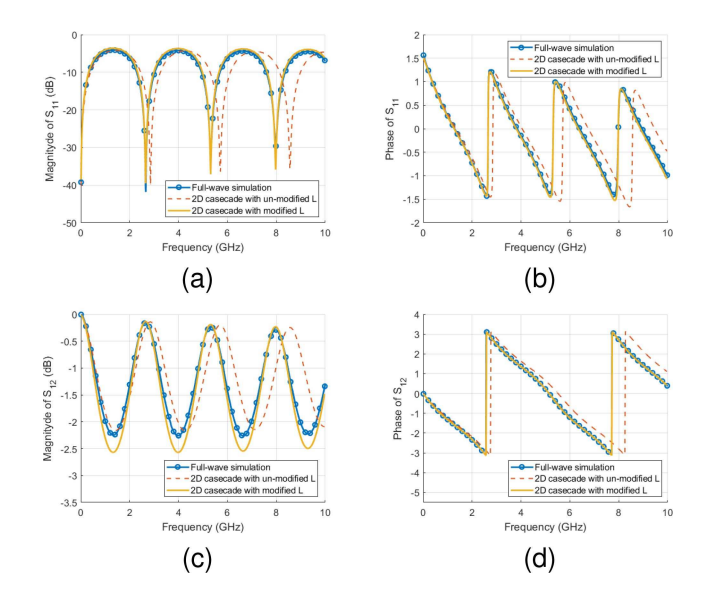


Fig. 14. Comparison between full-wave and segmented models. (a) Magnitude of S_{11} . (b) Phase of S_{11} . (c) Magnitude of S_{12} . (d) Phase of S_{12} .

where μ_0 is the permeability of free space, r is the distance from the observation point to the current source, and $\hat{e_{\varphi}}$ is the unit vector in the azimuthal direction (tangential to the circle with the center at the filament location and going through the observation point).

The magnetic flux through the surface S between the trace and the return plane generated by the ith filament can be expressed as

$$\Phi_i = \int_S \vec{B_i} \cdot d\vec{s}. \tag{28}$$

The surface S is defined between the edges of the signal trace and the return plane, as shown in Fig. 10. The distances from the ith filament to the edge of the return plane and the signal trace are denoted as d_{1i} and d_{2i} , respectively. Be defining a circle with the center of the filament and the radius equal to d_{2i} , it is possible to define surface S' which lies in the same plane as the filament. Since the \vec{B} field generated by the filament is tangential to the circle [see (27)] and the divergence of the \vec{B} field is zero, the flux through surfaces S and S' is equal. Therefore, the magnetic flux can be calculated as follows:

$$\Phi_{i} = \int_{S} \vec{B}_{i} \cdot d\vec{s} = \int_{S'} \vec{B}_{i} \cdot d\vec{s}'$$

$$= \int_{d_{1i}}^{d_{2i}} |\vec{I}_{i}| \frac{\mu_{0} dl}{2\pi x} dx = |\vec{I}_{i}| \frac{\mu_{0} dl}{2\pi} \ln \left(\frac{d_{2i}}{d_{1i}} \right) \tag{29}$$

where dl corresponds to the length of the segment in the z direction.

The total magnetic flux generated by all n return plane filaments is given by the sum of the contributions from each filament, which can be expressed as

$$\Phi_{\text{GND}} = \sum_{i=1}^{n} \Phi_i = \sum_{i=1}^{n} |\vec{I}_i| \frac{\mu_0 dl}{2\pi} \ln \left(\frac{d_{2i}}{d_{1i}} \right).$$
 (30)

The return plane inductance contribution is the ratio of the flux (30) to the total current

$$L_{\text{GND}} = \frac{\Phi_{\text{GND}}}{I} = \frac{1}{I} \sum_{i=1}^{n} |\vec{I}_{i}| \frac{\mu_{0} dl}{2\pi} \ln \left(\frac{d_{2i}}{d_{1i}}\right).$$
(31)

To find the inductance contribution in the case of the meshed ground, the contributions of each filament in (31) has to be modified according to (23)

$$L'_{\text{GND}} = \frac{1}{I} \sum_{i=1}^{n} |\vec{I}_i| \frac{\mu_0 dl}{2\pi} \ln \left(\frac{d_{2i}}{d_{1i}} \right) \frac{1}{\cos \theta_i}$$
 (32)

where θ_i is the angle of the current flow of the *i*th filament.

Similarly, the trace current can be treated as a combination of m filaments in the trace conductor. As show in Fig. 11, the inductance contribution of the trace $L_{\rm trace}$ in (26) can be calculated as

$$L_{\text{trace}} = \frac{\Phi_{\text{trace}}}{I} = \frac{1}{I} \sum_{i=1}^{n} |\vec{I_j}| \frac{\mu_0 dl}{2\pi} \ln\left(\frac{d_{2j}}{d_{1j}}\right)$$
(33)

where $\vec{I_j}$ is the current of the jth filament, d_{1j} and d_{2j} are the distance from the jth filament to the edge of the return plane and trace, as shown in Fig. 10. The total PUL inductance is calculated as

$$L' = L_{\text{trace}} + L'_{\text{GND}}.$$
 (34)

IV. VALIDATION OF THE PROPOSED METHOD

A. Trace Aligned With the Aperture Center

The proposed methodology was applied to the model depicted in Fig. 1, where the trace is aligned with the center of the return plane aperture. Following the completion of the 2-D analysis, the direction of the return current was reconstructed using the process described in Section III-A, as illustrated in Fig. 12.

Subsequently, the value of the PUL L was modified according to (32). The resulting dependency of the PUL inductance on the position along the TL is shown in Fig. 13. By combining the modified PUL L with the PUL RGC obtained directly from the 2-D analysis, the S-parameters of each segment were calculated.

Finally, the S-parameters of the entire board were obtained by cascading these segments together, as presented in Fig. 14. Using (1) and (2), the relative errors in the magnitude and phase of the transmission coefficient were 2% and 0.2%, respectively. It can be observed that after modifying the PUL L based on the return current direction, the cascaded results exhibit a much better correlation with the results of the full-wave simulation in terms of phase delay, as a consequence the magnitude error reduced as well because of the alignment of the nulls.

B. Trace Not Aligned With the Aperture Center

The proposed method can also be applied to cases where the trace is not aligned with the center of the apertures. To demonstrate this, the trace of the transmission line in Fig. 1 was shifted toward the positive x direction by 0.35 mm, as illustrated in Fig. 15. The region between the two black dashed

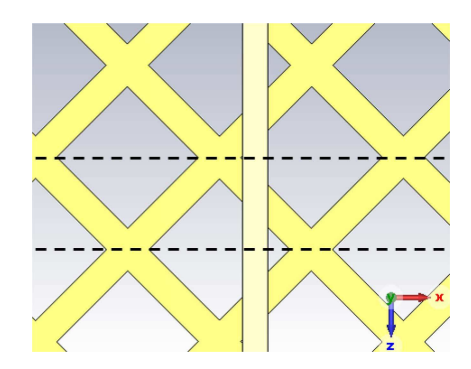


Fig. 15. Model with the trace off away from the aperture center. Only the portion close to the signal trace is shown.

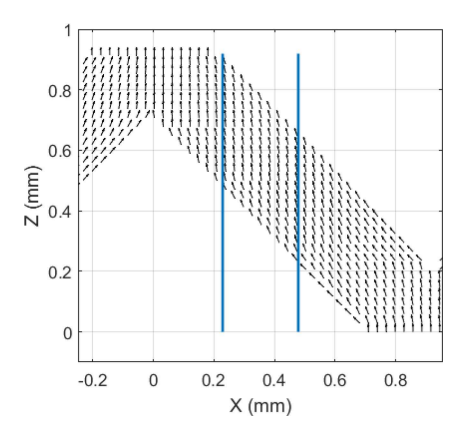


Fig. 16. Reconstructed return current direction. The blue lines indicate the position of the signal trace.

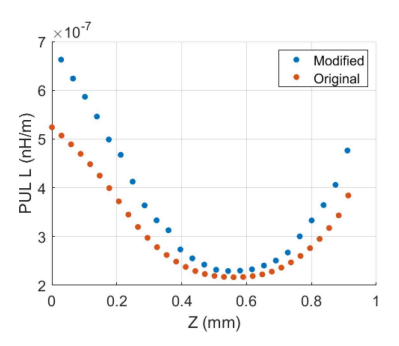


Fig. 17. PUL L before and after modification.

lines represents the half period of the meshed plane. Similar to the previous example, the model was cross-sectioned at the same 32 locations. Using the current magnitude distribution obtained from the 2-D analysis, the return current flow direction was reconstructed, as depicted in Fig. 16. The comparison between the PUL L obtained from the 2-D analysis and the modified result is shown in Fig. 17. By cascading the RLGC parameters of all segments together, the resulting S-parameters were calculated and presented in Fig. 18. A good correlation was achieved between the cascaded result and the full-wave simulation, indicating the effectiveness of the proposed methodology in such cases as well.

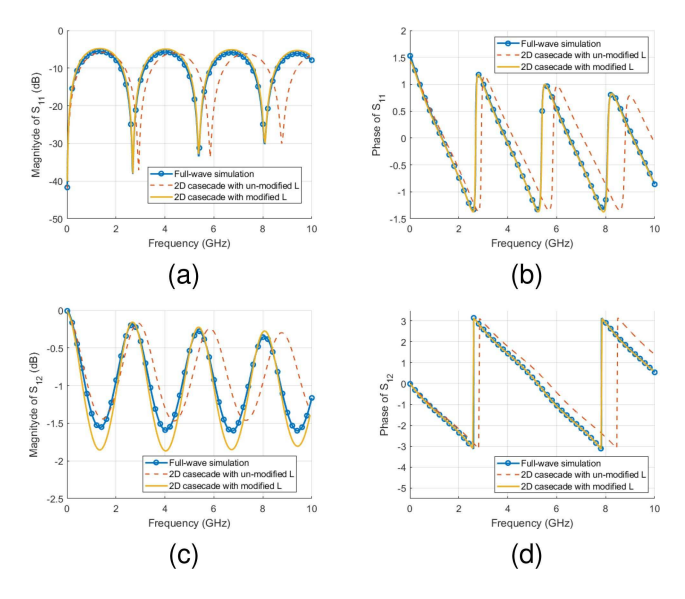


Fig. 18. Comparison between full-wave and segmented models. (a) Magnitude of S_{11} . (b) Phase of S_{11} . (c) Magnitude of S_{12} . (d) Phase of S_{12} .

V. CONCLUSION

The widespread use of FPCBs in contemporary electronic devices has made it increasingly important to accurately characterize transmission lines referenced to mesh return planes. In this article, a novel and efficient method is proposed for calculating the S-parameters of single-ended traces referenced to a meshed return plane using 2-D analysis.

Traditional 2-D cross-sectional analysis is inadequate for accurately characterizing transmission lines with meshed reference planes due to the geometry-induced changes in return current flow direction. The proposed approach addresses this limitation by considering the changes in the geometry and the position-dependent direction of current flow. The calculated inductance of the return plane obtained by the 2-D analysis was modified, effectively accounting for the current flow path around the mesh openings.

The validity of the approach was demonstrated through the modeling of transmission lines with both aligned and offset signal traces relative to the apertures in the meshed return plane. The proposed method yields consistent phase values for the reflection and transmission coefficients when compared to full-wave 3-D simulations. This correlation was crucial for accurately predicting skew and signal distortion during signal integrity analysis. Moreover, the magnitude of the S-parameters can be reasonably reconstructed, with a maximum error of approximately 0.3 dB. This aspect will be investigated in future studies.

In addition to the two validation cases demonstrated within this article, wherein the signal traces are aligned parallel to the diagonal axis of the mesh apertures, it is important to recognize that in practical applications, signal traces may assume an angle relative to this diagonal axis. In such scenarios, the angle formed between the signal trace and the diagonal axis of the mesh aperture determines the structure's periodicity and might require to increase the number of the cross sections (for the same cross-sectioning step). Nevertheless, the proposed method remains fully applicable.

In conclusion, this research carries significant implications for the design and optimization of FPCBs, contributing to the ongoing advancement of modern electronic devices.

REFERENCES

- S. H. Hall and H. L. Heck, Advanced Signal Integrity for High-Speed Digital Designs. Hoboken, NJ, USA: Wiley, 2011.
- [2] C. Wu, Z. Sun, Q. Huang, Y. Wang, J. Fan, and J. Zhou, "A method to extract physical dipoles for radiating source characterization and near field coupling estimation," in *Proc. IEEE Int. Symp. Electromagn. Compat.*, *Signal Power Integrity*, 2019, pp. 580–583.
- [3] Z. Sun, Y. Wang, W. Lee, K. Wu, and D. Kim, "Radiated noise source characterization based on magnitude-only near field," in *Proc. IEEE Int. Joint EMC/SI/PI EMC Europe Symp.*, 2021, pp. 376–380.
- [4] D. M. Pozar, Microwave Engineering. Hoboken, NJ, USA: Wiley, 2011.
- [5] Z. Sun, J. Liu, X. Xiong, V. Khilkevich, D. Kim, and D. Beetner, "Extraction of stripline surface roughness using cross-section information and s-parameter measurements," in *Proc. IEEE Int. Symp. Electromagn. Compat. Signal/Power Integrity*, 2022, pp. 80–85.
- [6] J. He et al., "Extracting characteristic impedance of a transmission line referenced to a meshed ground plane," in *Proc. IEEE Int. Symp. Electromagn. Compat.*, 2016, pp. 651–656.
- [7] F. Xiao, K. Murano, and Y. Kami, "Modeling of differential line referenced to a meshed ground plane," in *Proc. Int. Symp. Electromagn. Compat.*, 2014, pp. 735–740.
- [8] S. Wu, H. Shi, M. Herndon, B. Cornelius, M. Halligan, and J. Fan, "Modeling and analysis of a trace referenced to a meshed ground plane," in *Proc. IEEE Int. Symp. Electromagn. Compat.*, 2011, pp. 137–141.
- [9] CST Studio Suite 3D EM simulation and analysis software, Dassault Systemes Simulia Corp. Accessed: Dec. 18, 2022.
- [10] J. Fan, X. Ye, J. Kim, B. Archambeault, and A. Orlandi, "Signal integrity design for high-speed digital circuits: Progress and directions," *IEEE Trans. Electromagn. Compat.*, vol. 52, no. 2, pp. 392–400, May 2010.
- [11] E. M. Purcell and D. J. Morin, *Electricity and Magnetism*. Cambridge, U.K.: Cambridge Univ. Press, 2013.
- [12] K. W. Morton and D. F. Mayers, Numerical Solution of Partial Differential Equations: An Introduction. Cambridge, U.K.: Cambridge Univ. Press, 2005.
- [13] C. R. Paul, Analysis of Multiconductor Transmission Lines. Hoboken, NJ, USA: Wiley, 2007.
- [14] B. I. Bleaney, B. I. Bleaney, and B. Bleaney, Electricity and Magnetism, vol. 2. London, U.K.: Oxford Univ. Press, 2013.
- [15] C. R. Paul, Inductance: Loop and Partial. Hoboken, NJ, USA: Wiley, 2011.
- [16] A. E. Ruehli, "Inductance calculations in a complex integrated circuit environment," *IBM J. Res. Develop.*, vol. 16, no. 5, pp. 470–481, 1972.
- [17] R. A. Serway and J. W. Jewett, Physics for Scientists and Engineers. Boston, MA, USA: Cengage Learning, 2018.